Automated tongue segmentation in hyperspectral images for medicine

Zhi Liu,[1] Jing-qi Yan,[1] David Zhang,[2,*] and Qing-Li Li[3]

[1]Institute of Image Processing and Pattern Recognition, Shanghai Jiao Tong University, Shanghai, China
[2]Department of Computing, the Hong Kong Polytechnic University, Hong Kong, China
[3]School of Information Science, East China Normal University, Shanghai, China

*Corresponding author: csdzhang@comp.polyu.edu.hk

Automatic tongue area segmentation is crucial for computer aided tongue diagnosis, but traditional intensity-based segmentation methods that make use of monochromatic images cannot provide accurate and robust results. We propose a novel tongue segmentation method that uses hyperspectral images and the support vector machine. This method combines spatial and spectral information to analyze the medical tongue image and can provide much better tongue segmentation results. The promising experimental results and quantitative evaluations demonstrate that our method can provide much better performance than the traditional method. © 2007 Optical Society of America

OCIS codes: 100.5010, 100.2960, 170.4580, 170.6510.

1. Introduction

Techniques such as magnetic resonance imaging (MRI), computer tomography (CT), and ultrasound have dramatically promoted the development of modern biomedical engineering [1]. Among many research problems in biomedical engineering, image segmentation is still a challenging field for researchers, mainly because of the ambiguity between the organ and its ambient tissues. This difficulty becomes especially harder under the living dynamic situation, since the squirm of the organ will deteriorate the detection. A typical example is the human tongue.

The human tongue is a unique organ that can be stuck out of the body for inspection. So it plays an important role not only in the diagnosis of tongue cancer [2] and glossitis [3], but also in tongue diagnosis of traditional Chinese medicine (TCM) [4]. However, tongue segmentation for computer-aided diagnosis is hard work resulting from the human tongue's physiological properties. First, there are some ravines and patches on the surface of the tongue that have a significant influence on edge detection.

Second, people can stick out only a part of the tongue, and there are no criteria on the quantity of the part. In other words, the part of the tongue that we can inspect is random. Third, according to TCM, [5] the color, plumpness, and slenderness of the tongue can vary because of disease. In recent years, some researchers were attracted to this work [4,6]. However, these methods are not always effective [4], especially when the surface color of the tongue is similar to its ambient tissue. The reason for this limitation is mainly that all methods are based on the analysis of intensity difference in monochromatic images, which inspires us to exploit other more effective methods.

A. Hyperspectral Imaging and Its Advantages

The increasing requirement for accurate noninvasive diagnosis and treatment promotes the application of optical technologies in this field. Optical techniques have the ability to perform a diagnosis on tissues without the need for sample excision. Another advantage of optical diagnosis is that the resulting information can be available visually. Current optical diagnostic technologies can be categorized into three broad categories. The first, which records a two-dimensional (2D) image of an area of the sample of interest at one specific wavelength, can be called an

optical image (OI). The second, which obtains an entire spectrum of a single tissue within a wavelength region of interest, can be called a spectral image (SI). The third is relatively new, combines the two modalities mentioned above, and is often referred to as hyperspectral imaging (HSI) [7].

Use of HSI for biomedical applications is attractive, since it records the entire emission for every pixel on the entire image in the field of view [8]. It is well known that the interaction of light with human tissue varies, which has been studied extensively by researchers [9,10]. Small changes in the distribution of pigments such as melanin, hemoglobin, bilirubin, and β-carotene in the epidermal and dermal layers of the human skin can produce significant changes in the skin's spectral reflectance [11]. Some researchers [12,13] measured skin reflectance spectra over the visible wavelengths and modeled them. For instance, Angelopoulou *et al.* [12] used a skin reflectance model to propose a method for skin detection under varying lighting conditions.

The automatic segmentation of anatomical structures in traditional monochromatic images is often performed using model-based nonrigid registration methods. That is to say, an automatic segmentation of a certain structure can be obtained by registering a labeled model, typically generated in a manual segmentation process, to another data set containing the structure of interest. This registration is difficult and laborious [14]. This is a problem that might be solved if the variability in the spectra of different tissue types could be used to distinguish between the human tongue and the nontongue biological substances in hyperspectral image space.

B. Support Vector Machines for Hyperspectral Image Analysis

Many supervised methods have been developed to classify both multispectral data. Some of the successful approaches to multispectral data classification have used artificial neural networks, such as multilayer perceptrons (MLPs) [16] and radial basis function neural networks (RBFNNs) [17]. However, these approaches are not effective when dealing with a large number of spectral bands since they are highly sensitive to the Hughes phenomenon [18] known as the curse of dimensionality. That is, for a fixed and finite number of training samples, with the number of features increasing, the classification accuracy first improves to a peak value and then declines. The decline is due to limitations on the precision of class statistics estimation resulting from limited training data. Fortunately, support vector machines (SVM) [18] can conquer the curse of dimensionality. In recent years, SVM has been successfully used for the classification of hyperspectral data [15]. It has three advantages: (1) large input spaces are available for SVM; (2) SVM is robust against noise; and (3) SVM generates sparse solutions, which are subsets of training samples.

We provide a novel framework for tongue area segmentation that uses the hyperspectral images acquired with our special device and the supervised SVM classifier. This approach combines the spectral and spacial information of the tongue surface and presents promising results for further analysis.

C. Organization of this Paper

The remainder of the paper is organized as follows. In Section 2 we describe the setup of the device. In Section 3 briefly introduce SVMs. We describe the segmentation framework in Section 4 and the experimental results and quantitative evaluations in Section 5. Our conclusions are presented in Section 6.

2. Setup of the Device

To obtain the hyperspectral image data, the device based on the theory of the pushbroom hyperspectral imager (PHI) [19,20] is used, whose main modules are illustrated in Fig. 1. It consists of a spectrometer, a matrix CCD, an instrument translation module, and a data collection module. This device has the ability to acquire a complete spatial-spectral image cube in 180 ms from 400 to 1000 nm, which basically eliminates motion artifacts. We built a studio with two constant light sources for this capture device so that the illumination is constant. Each of the light sources is a 100 W halogen lamp with a white diffuser screen. The two sources provide approximately uniform illumination on the subject. Also, the camera has been calibrated and fixed on the frame. The distance between the lens and the tongue is constant, and the head of the patient can be constrained by a framework (shown in Fig. 6). Therefore, the illumination can be considered to be constant in our study.

This device provides a sequence of images in different spectral bands. In other words, the HSI approach provides a "data cube" of spectral information, that consists of a series of optical images recorded at various wavelengths of interest. An example of the image cube is illustrated in Fig. 2. Each pixel of the image has two properties; the spectrum property and the intensity property. Based on analyzing the "image cube," we can see that different object surfaces can be represented by different band curves. Thus, using these special tongue images, we can do tongue area segmentation according to the difference in spectral curves between the tongue and its ambient organs.
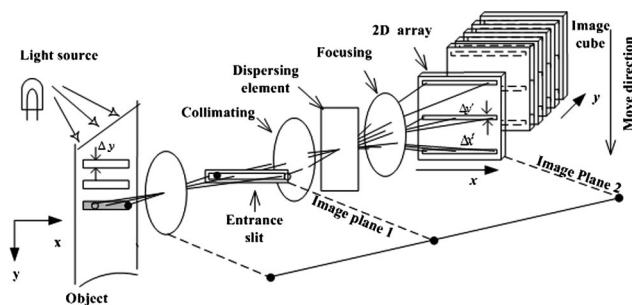

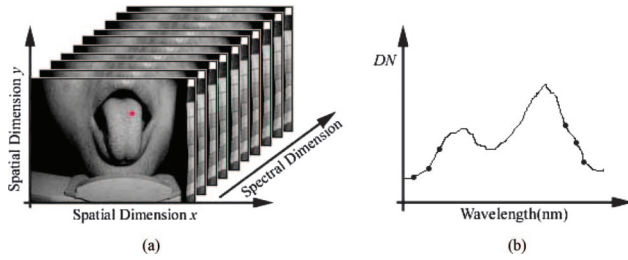Fig. 1. Schematic of hyperspectral imaging sensor system.

Fig. 2. (Color online) (a) HSI cube and (b) spectrum corresponding to the point in (a).

Fig. 3. Flow chart of hyperspectral tongue image segmentation procedure.

3. Description of Support Vector Machines

The SVM is a popular classifier based on statistical learning theory as proposed by Vapnik [22]. The training phase of SVMs is to find a linear optimal separating hyperplane as a maximum margin classifier with respect to the training data. In SVMs, support vectors, which are critical for classification, are obtained in a learning phase that uses training samples. In the test phase for classification, class labels are found for the new (i.e., unknown) feature vectors using support vectors. When the training data are not linearly separable, the kernel methods [23] are used in SVMs. These kernel methods map data from the original input space to a kernel feature space of higher dimensionality. The parameters of the kernels are important for the classification results. In contrast to the traditional learning methods, a SVM does not depend explicitly on the dimensionality of input spaces so it is a good candidate for a supervised classification of hyperspectral images. Some references [18,22,23] detailed the information about SVM.

4. Segmentation Framework

As hyperspectral images can provide both spectral and spatial information to identify and distinguish specific materials, our method integrates HSI with SVM for tongue area segmentation. The process begins with the calibration for hyperspectral images, then, the region of interest is determined. After the input data are normalized, the SVM is used for classification. At last, according to the results of classification, we obtain the contour of the tongue. The pipeline of the procedure is illustrated in Fig. 3, and its main modules are described in the following.

A. Hyperspectral Image Calibration

To obtain the unified representation of the reflectance values for computing, it is necessary to calibrate the raw hyperspectral images first. An effective method for calibration has been presented by Pan and Healey [13], which we describe briefly as follows.

This method acquires two additional images in black and white. The black image, which has near 0% reflectance, can be obtained by covering the lens. The white image refers to near totally reflected image and is acquired with a white panel in front of the camera at the same distance for human tongue acquisition.
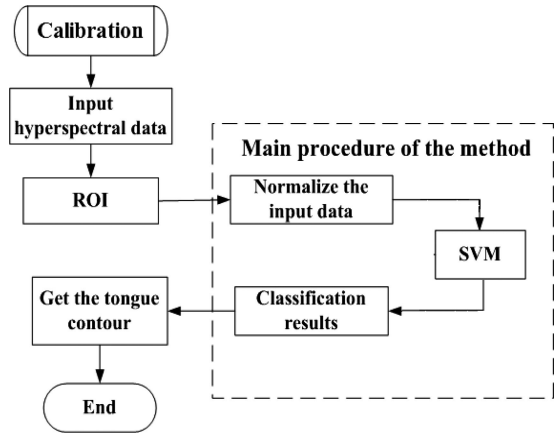
The calibration is traceable to the U.S. National Institute of Standards and Technology (NIST) [13].

The image intensity at the spatial coordinate (x, y) for wavelength λ_i can be modeled as

$$I(x, y, \lambda_i) = L(x, y, \lambda_i)S(x, y, \lambda_i)R(x, y, \lambda_i) + O(x, y, \lambda_i), \tag{1}$$

where $L(x, y, \lambda_i)$ refers to the illumination, $S(x, y, \lambda_i)$ refers to the system spectral response, $R(x, y, \lambda_i)$ refers to the reflectance of the viewed surface, and $O(x, y, \lambda_i)$ refers to the offset, which includes dark current and stray light. $i = \{1, 2, \ldots, b\}$, b is the number of spectral bands (in our study, $b = 120$).

For the white image, the intensity of coordinate (x, y) for wavelength λ_i can be modeled as

$$I_W(x, y, \lambda_i) = L(x, y, \lambda_i)S(x, y, \lambda_i)R_W(x, y, \lambda_i) + O(x, y, \lambda_i), \tag{2}$$

and for the black image, the intensity of coordinate (x, y) for wavelength λ_i can be modeled as

$$I_B(x, y, \lambda_i) = L(x, y, \lambda_i)S(x, y, \lambda_i)R_B(x, y, \lambda_i) + O(x, y, \lambda_i), \tag{3}$$

where $R_W(x, y, \lambda_i)$ and $R_B(x, y, \lambda_i)$ are reflectance functions of the white image and the black image, respectively. Since the viewed surfaces have the same reflectance property for all image pixels, $R_W(x, y, \lambda_i)$ and $R_B(x, y, \lambda_i)$ are theoretically independent of (x, y) and can be denoted as $R_W(\lambda_i)$ and $R_B(\lambda_i)$.

Combining Eqs. (2) and (3), we can estimate $L(x, y, \lambda_i)S(x, y, \lambda_i)$ as

$$L(x, y, \lambda_i)S(x, y, \lambda_i) = \frac{I_W(x, y, \lambda_i) - I_B(x, y, \lambda_i)}{R_W(\lambda_i) - R_B(\lambda_i)}. \tag{4}$$

When Eq. (4) is substituted into Eq. (3), $O(x, y, \lambda_i)$ can be estimated as

$$O(x, y, \lambda_i) = I_B(x, y, \lambda_i) - \frac{I_W(x, y, \lambda_i) - I_B(x, y, \lambda_i)}{R_W(\lambda_i) - R_B(\lambda_i)}$$
$$\times R_B(\lambda_i). \tag{5}$$

With Eqs. (4) and (5), we obtain the calibration equation provided below:

$$R(x, y, \lambda_i) = \frac{I(x, y, \lambda_i) - I_B(x, y, \lambda_i)}{I_W(x, y, \lambda_i) - I_B(x, y, \lambda_i)} R_W(\lambda_i)$$
$$+ \frac{I_W(x, y, \lambda_i) - I(x, y, \lambda_i)}{I_W(x, y, \lambda_i) - I_B(x, y, \lambda_i)} R_B(\lambda_i). \tag{6}$$

B. Segmentation

The process of segmentation is begun by selecting the region of interest (ROI), which eliminates the background from the original images (shown in Fig. 4). Thus, the primary sources of variance in the input data, which are the intensity and spectral curve shape, are limited to five classes; i.e., the tongue, the face, the lip, the teeth, and the tissues of the inner mouth. We represent each tongue image using the feature vectors that are extracted from the ROI. The feature vector at coordinate (x, y) can be denoted as $R = [r(x, y, \lambda_1), r(x, y, \lambda_2, \ldots, r(x, y, \lambda_b)]^T$, where $r(x, y, \lambda_i)$ denotes the reflectance at λ_i, and b is the number of spectral bands (in our study, $b = 120$). Then, the normalized spectral reflectance vector $\tilde{R}$ is defined by

$$\tilde{R} = R/\|R\|, \tag{7}$$

where $\|\cdot\|$ means the L_2 norm.

Here we should note that in this study the feature vectors are composed of the reflectance values at all wavelength bands. This is because the SVM that we used for classification is different from the traditional classifiers that suffer from the curse of dimensionality [18], such as MLP [16], and RBFNN [17]. As a superior classification algorithm, SVM works well on hyperspectral data and does not require preprocessing to reduce data dimensionality for conquering the curse of dimensionality [15]. In fact, we have found that the accuracy of SVM deteriorates with the application of feature extraction techniques [21]. This demonstrates that for SVM classification, the possibility of finding an optimum hyperplane for separating the classes is higher in the high dimensional data set than in the reduced dimensionality data set.

Fig. 4. ROI in the captured image (the left) and the binary image representing the detected tongue area (the right).
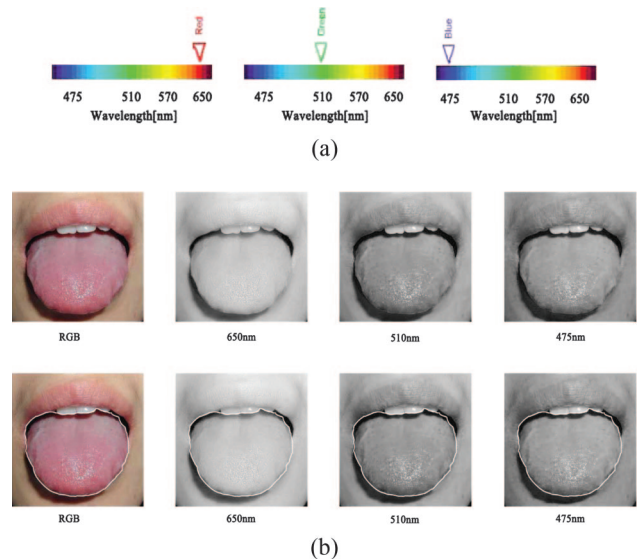
Fig. 5. (Color online) (a) Spectrum of the visible light. (b) Top row: RGB tongue image synthesized by three spectral images. Bottom row: segmentation results in hyperspectral images and mapping them directly into the RGB tongue image.

Therefore, unlike other classifiers, SVM classifiers may be adopted when the entire data set is required to be used, and so, in our study we have selected all the wave bands as the input features for classification.

The next step is to use the SVM to classify the tongue and nontongue areas. To do this, the input feature space is first mapped by a kernel transformation into a higher dimensional space, where it is expected to find a linear separation that maximizes the margin between the two classes. In the hyperspectral space, a normally distributed model is a reasonable assumption for optical human organ detection data. A number of kernels have been discussed for the SVM, but it is not clear how to choose one that gives the best generalization for a particular problem. The type of kernel that is chosen and the values of the parameters associated with the kernel both affect the classification accuracy. In our study, the popular Gaussian kernel is exploited for the SVM, and the multiclass strategy for the SVM [14] is used to classify the various tissues. SVM labels the separated parts as tongue, face, lip, teeth, and the inner tissue of the mouth. Then the pixel of the tongue area is represented by "1" and that of the nontongue area is represented by "0" in a corresponding binary image of the same size (Fig. 4) extracting the contour of the tongue. Finally, we map the results into the color tongue images (see Fig. 5). Note these color images are in red-green-blue (RGB) color space and can be integrated using three frames from a hyperspectral image cube corresponding to 650 nm (red), 510 nm (green), and 475 nm (blue).

5. Experiments and Comparisons

We used our hyperspectral image capture device to obtain a series of tongue images with the efficient
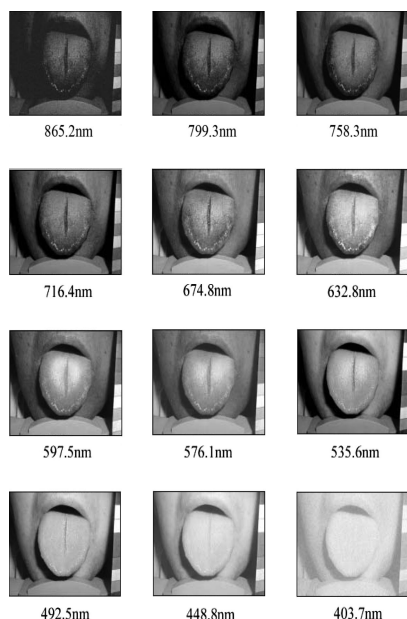
Fig. 6. Series of visible spectral tongue images from a hyperspectral image cube.

Fig. 8. Block diagram of the architecture for solving multiclass problems with SVMs.

In the following subsections, we propose the criteria of evaluation and compare our approach with the popular method called bi-elliptical deformable contour (BEDC).

A. Criteria of Evaluation

It is necessary to evaluate the performance of the segmentation quantitatively. Chalana and Kim [24] suggested the use of boundary error metrics to evaluate segmentation performance. Let $A = \{a_1, a_2, \ldots, a_m\}$ and $B = \{b_1, b_2, \ldots, b_n\}$ denote the automatic segmentation result and manual segmentation result, respectively, where $a_1, a_2, \ldots, a_m$ and $b_1, b_2, \ldots, b_n$ are points on the corresponding boundary curve. Define the distance to the closest point (DCP) for a_i to curve B as

$$d(a_i, B) = \min_j \|b_j - a_i\|. \tag{8}$$

Then, the Hausdorff distance (*HD*) between the two curves is defined as the maximum of the DCP between the two curves. This can be formularized as

$$HD(A, B) = \max\left(\max_i\{d(a_i, B)\}, \max_j\{d(b_j, A)\}\right). \tag{9}$$

The mean DCP distance (*MD*) of two curves A and B can be defined as

$$MD(A, B) = \frac{1}{m+n}\left(\sum_i d(a_i, B) + \sum_j d(b_j, A)\right). \tag{10}$$

B. Comparison with BEDC

To our best knowledge, BEDC proposed by Pang *et al.* [4] is currently the most effective method for use in tongue segmentation applications. BEDC combines a bi-elliptical deformable template (BEDT) and an active contour model. The BEDT captures gross shape features by using the steepest descent method on its energy function in the parameter space. The BEDC is derived from the BEDT by substituting template forces for classical internal forces and can deform to fit local details. However, this method is based on the intensity of images and cannot get satisfactory results when the intensity values of the tongue and its ambient tissues are close [4]. Our HSI+SVM method combines the hyperspectral image spectral features and the effective classifier, SVM, to segment

pixels of 652×488. The device was operated in a spectral wavelength range of 400–1000 nm with two distinct spectra regimes, visible (400 and 720 nm) and near infrared (720 and 1000 nm). One hundred and fifty-two volunteers were sampled for this experiment. Figure 6 shows some examples of the captured images from the visible wavelength range at different bands, and Fig. 7 illustrates the differences in the spectral curves of different tissues. Eighty samples were randomly chosen from 152 volunteers and were used to train SVMs, and the remainders were used for testing. In this experiment, for training, we manually extracted from the training sample set samples of the tongue, face, teeth, lip, and tissue of inner mouth. We used a "one-against-all" multiclass strategy [15]. This very common approach is based on a parallel architecture made up of T ($T = 5$ in our study) SVMs. Each SVM solves a two-class problem defined by one class against all the others. The "winner-takes-all" rule is used for the final decision. That is, the winning class is the one corresponding to the SVM with the highest output (discriminant function value). The architecture of this strategy can be seen in Fig. 8.
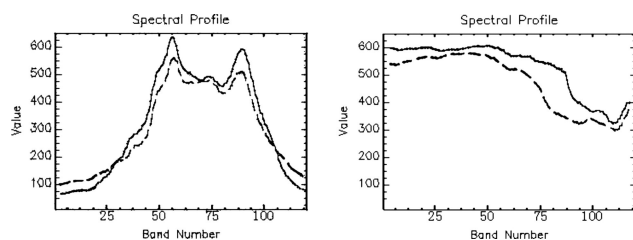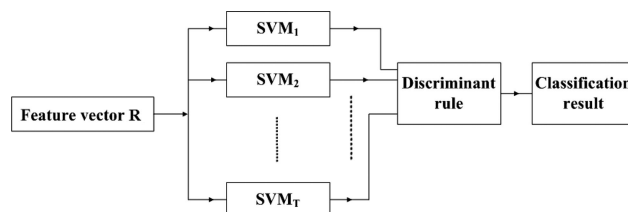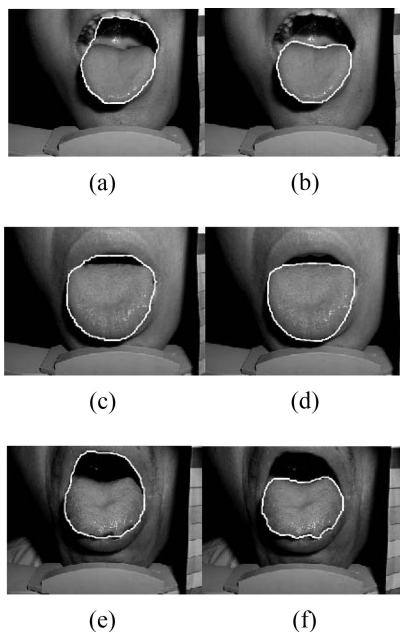

Fig. 7. Spectral curves of the tongue and the skin of the face from two subjects.

(a)   (b)

(c)   (d)

(e)   (f)

Fig. 9. Comparison of tongue segmentation results (a). (c) and (e) are the results of the BEDC method [4]. (b), (d), and (f) are the results of our proposed HSI+SVM method.

the tongue area, which is immune to the factors that affect the performance of BEDC. Figure 9 shows some results of segmentation using our method and BEDC. The results of HSI+SVM are shown in Figs. 9(b), 9(d), and 9(f). We implement the BEDC algorithm with the images at the spectral band whose central wavelength is 492.5 nm. The results of BEDC can be seen in Figs. 9(a), 9(c), and 9(e).

We evaluated the segmentation performance of HSI+SVM and BEDC using the distance measurement mentioned in Subsection 5.A. To calculate the distance, we manually extracted the ground truths (i.e., the accurate boundaries of the tongue) from the images. We then calculated the distance between the ground truth and the results using HSI+SVM and BEDC, respectively. For the distance measure, we use HD and MD defined by Eqs. (9) and (10). $\overline{HD}$ and $\overline{MD}$ as shown in Table 1 are both the average of the testing results, which can be formularized as

$$\overline{HD} = \sum_{i=1}^{N} HD/N \quad \overline{MD} = \sum_{i=1}^{N} MD/N, \quad (11)$$

where N is the number of the testing examples (in our study, $N = 152 - 80 = 72$). Furthermore, we show the standard error (S_E) of HD and MD that we used

Table 1. Comparison of HSI+SVM Method and the BEDC Method [4] Tongue Segmentation Results in Terms of Boundary Metrics

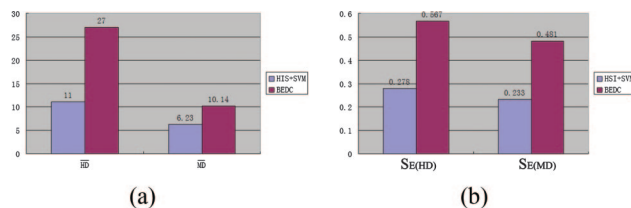|	HD (in pixels)	$S_{E(HD)}$	MD (in pixels)	$S_{E(MD)}$
HSI+SVM	11	0.278	6.23	0.233
BEDC [4]	27	0.567	10.14	0.481

(a)   (b)

Fig. 10. (Color online) Histogram of the comparison of our method and BEDC: (a) $\overline{HD}$ and $\overline{MD}$ and (b) $S_{E(HD)}$ and $S_{E(MD)}$.

in comparing our method and BEDC. The standard error can be computed as

$$S_E = \frac{s}{\sqrt{N}}, \quad s = \sqrt{\frac{1}{N-1}\sum_{i=1}^{N}(x_i - \bar{x})^2}, \quad (12)$$

where s is the sample standard deviation.

Table 1 and Fig. 10 show the results of the comparison of our method and BEDC. We can see that the values of $\overline{HD}$ and $\overline{MD}$ with our method are 11 and 6.23, respectively. In contrast, the two values of BEDC are 27 and 10.14, respectively. It is obvious that our method produces more accurate results than BEDC. Furthermore, the standard errors of HD and MD when we use our method are both much smaller than those of BEDC. This shows that our method can obtain more stable segmentation results than BEDC.

6. Conclusion

In the field of human tongue segmentation, traditional deformable template methods are popular. However, these intensity-based algorithms are not always robust, as in a monochromatic image, the intensity of the surface of the tongue may be similar to that of surrounding tissue. We have presented what we believe to be a new method for segmenting medical images of the tongue. The method (HSI+SVM) uses hyperspectral images to differentiate between the tongue and the surrounding tissue by exploiting the spectral variability of different tissue types and combines it with support vector machines, a popular classifier that does not depend explicitly on the dimensionality of input spaces and has a good generalization performance. The experimental result and the corresponding quantitative evaluation demonstrate that the proposed hybrid HSI+SVM approach can provide more effective and robust performance than the traditional method.

References

1. T. Vo-Dinh, ed., *Biomedical Photonics Handbook* (CRC, 2003).
2. R. B. Bell, D. Kademani, L. Homer, E. J. Dierks, and B. E. Potter, "Tongue cancer: is there a difference in survival compared with other subsites in the oral cavity?" J. Oral Maxillofac. Surg. **65,** 229–236 (2007).
3. J. A. Byrd, A. J. Bruce, and R. S. Rogers, "Glossitis and other tongue disorders," Dermatol. Clin. **21,** 123–134 (2003).
4. B. Pang, D. Zhang, and K. Q. Wang, "The bi-elliptical deformable contour and its application to automated tongue segmentation in Chinese medicine," IEEE Trans. Med. Imaging **24,** 946–956 (2005).
5. I. Feng and S. Tianbin, *Practicality handbook of tongue diagnosis of TC (in Chinese)* (Ke Xue Chu Ban She, 2002).
6. W. Zuo, K. Wang, D. Zhang, and H. Zhang, "Combination of polar edge detection and active contour model for automated tongue segmentation," in *Proceedings of Third International Conference on Image and Graphics* (IEEE, 2004), pp. 270–273.
7. T. Vo-Dinh, "A hyperspectral imaging system for in vivo optical diagnostics," IEEE Eng. Med. Biol. Mag. **23,** 40–49 (2004).
8. N. Magotra, E. Wu, P. Soliz, P. Truitt, P. Gelabert, and T. Stetzler, "Hyperspectral biomedical image formation," *Thirty-Third Asilomar Conference on Signals, Systems, and Computers* (IEEE, 1999), pp. 462–465.
9. V. Tuchin, *Tissue optics: light scattering methods and instruments for medical diagnosis* (SPIE Press, 2000).
10. R. Anderson and J. Parrish, "The Optics of Human Skin," J. Invest. Dermatol. **77,** pp. 13–19 (1981).
11. E. Edwards and S. Duntley, "The pigments and color of living human skin," Am. J. Anat. **65,** pp. 1–33 (1939).
12. E. Angelopoulou, R. Molana, and K. Daniilidis, "Multispectral skin color modeling," in *Proceedings of IEEE Conference on Computer Vision and Pattern Recognition* (IEEE, 2001), pp. 635–642.
13. Z. Pan and G. Healey, "Face recognition in hyperspectral images," IEEE Trans. Pattern Anal. Mach. Intell. **25,** pp. 1552–1560 (2003).
14. W. R. Crum, T. Hartkens, and D. L. G. Hill, "Non-rigid image registration: theory and practice," Br. J. Radiol. **77,** pp. S140–S153 (2004).
15. F. Melgani and L. Bruzzone, "Classification of hyperspectral remotesensing images with support vector machines," IEEE Trans. Geosci. Remote Sens. **42,** pp. 1778–1790 (2004).
16. H. Bischof and A. Leona, "Finding optimal neural networks for land use classification," IEEE Trans. Geosci. Remote Sens. **36,** pp. 337–341 (1998).
17. L. Bruzzone and D. Fernández-Prieto, "A technique for the selection of kernel-function parameters in RBF neural networks for classification of remote-sensing images," IEEE Trans. Geosci. Remote Sens. **37,** pp. 1179–1184 (1999).
18. G. E. Hughes, "On the mean accuracy of statistical pattern recognizers," IEEE Trans. Inf. Theory **14,** pp. 55–63 (1968).
19. P. Mouroulis, R. O. Green, and T. G. Chrien, "Pushbroom imaging spectrometer design for optimum recovery of spectroscopic and spatial information," Appl. Opt. **39,** pp. 2210–2220 (2000).
20. M. B. Sinclair, J. A. Timlin, D. M. Haaland, and M. Werner-Washburne, "Design, construction, characterization, and application of a hyperspectral microarray scanner," Appl. Opt. **43,** pp. 2079–2088 (2004).
21. C. A. Shah, P. Watanachaturaporn, P. K. Varshney, and M. K. Arora, "Some recent results on hyperspectral image classification," in *Proceedings of IEEE Workshop on Advances in Techniques for Analysis of Remotely Sensed Data* (IEEE, 2003), pp. 346–353.
22. V. N. Vapnik, *The Nature of Statistical Learning Theory* (Springer-Verlag, 1995).
23. G. Camps-Valls and L. Bruzzone, "Kernel-based methods for hyperspectral image classification," IEEE Trans. Geosci. Remote Sens. **43,** pp. 1351–1362 (2005).
24. V. Chalana and Y. Kim, "A methodology for evaluation of boundary detection algorithms on medical images," IEEE Trans. Med. Imaging **16,** pp. 642–652 (1997).